Experimental Evaluation of Nonisothermal Solid-Gas Reaction Model

The nonisothermal unreacted-core-shrinking model with unsteady state heat transfer analysis has been experimentally evaluated. The system studied is the combustion of a single agglomerated carbon-fire clay sphere in a thermobalance. By comparing the experimental results with those predicted by the model, it is concluded that the model adequately describes the reaction system under the experimental conditions such that the ash layer diffusion is rate controlling.

S. C. WANG and C. Y. WEN

Department of Chemical Engineering West Virginia University Morgantown, West Virginia 26506

SCOPE

In spite of a number of models proposed for noncatalytic solid-gas reactions, we seem to suffer from a lack of experimental data designed to test critically the existing models. This study presents an experimental evaluation of the validity of the unreacted-core-shrinking model. The combined effects of heat and mass transfer on chemical reaction during the combustion of an agglomerated carbon-fire clay ball under nonisothermal unsteady state conditions are examined. The validity of the pseudo-steady state assumptions is tested.

CONCLUSIONS AND SIGNIFICANCE

The combustion of a single carbon-fire clay sphere in the present study was describable by the unreacted-core-shrinking model at the reactor temperatures of 800°K or higher when the ash layer diffusion was rate controlling. Although the porosity of the unreacted core was fairly high ($\epsilon_0 = 0.40 \sim 0.50$), the unreacted-core-shrinking model did describe the reaction system successfully when the ash layer diffusion controlled the overall rate. When a gradual extinction occurs the unreacted-core model is no longer applicable after the extinction.

The pseudo-steady state assumption for heat transfer and the assumption that the unreacted core has uniform temperature are reasonable when the unreacted core and the product layer have high thermal diffusivities. Otherwise, significant deviation between the prediction and the actual performance will result during the initial period and during the transition of the rate controlling regime. This is especially true when the rate of heat generation is high as observed in the high-carbon content particle. The deviation during the initial period can be mostly avoided, however, by preheating the particle in an inert atmosphere before its entry to the reactor. The effective diffusivity measured directly agreed reasonably with that calculated from the model. The unreacted-core-shrinking model must be used with caution during the initial period and during the transition of the rate controlling regime.

Among the many noncatalytic solid-gas reaction models, two distinct types representing the limiting cases are a heterogeneous or unreacted-core-shrinking model, in which the reaction occurs at a reaction interface, and a homogeneous model where the reaction occurs uniformly throughout the interior of the solid.

A number of models dealing with the intermediate cases between the above two limiting cases have also been proposed. Various mathematical models useful for describing noncatalytic solid-fluid reaction systems were previously presented (Wen, 1968).

Since a number of cases observed can be approximated closely by the unreacted-core-shrinking model (Levenspiel, 1962), the present study will be based on this particular type of model.

As early as the late 1920s Ogawa (1929) applied the unreacted-core-shrinking model to analyze the diffusion problem when zinc sulphide was oxidized. Yagi and Kunii (1955) proposed a more general case of unreacted-core-shrinking model which accounted for the effects of diffusion across the gas film and diffusion through the solid product (ash) layer on the overall reaction rate. This model was later discussed by Levenspiel (1962). Weisz and Goodwin (1963) found that the model adequately describes the carbon burn-off in a catalyst at a sufficiently high temperature, based on the isothermal analysis.

A number of experimental studies based on Yagi and Kunii's unreacted-core-shrinking model, however, have presented contradicting conclusions with regard to the rate-controlling factors. Nearly all of these analyses have neglected the effect of the heats of reactions, which may have contributed to the disagreement.

Costa and Smith (1971) demonstrated the importance of temperature gradients inside the pellet in the hydrofluorination of uranium dioxide.

Correspondence concerning this paper should be addressed to C. Y. Wen. S. C. Wang is with Bechtel Corporation, 50 Beale Street, San Francisco, California 94119.

The effects of heat of reaction and heat transfer were investigated by Cannon and Denbigh (1957). In studying the oxidation of ZnS particles, they found that at above 900°C the formation of the ZnO layer became very uneven, developing a nonuniform surface of the unreacted core. They subsequently suggested that there were two types of thermal instabilities in the exothermic noncatalytic solid-gas reactions: unstable crossing of the curves of heat generation and heat loss, and the effect of solid product in impeding the loss of heat.

Shen and Smith (1965) discussed the metastable regime in the nonisothermal solid-gas reaction by means of heat balance equations under pseudo steady state approximation. They concluded that, for an exothermic reaction, the transition between the diffusion and kinetic regimes is possible during the course of reaction in a single particle. Approximate criteria were presented for the region of instability.

Aris (1967) showed that the approximate instability criteria of Shen and Smith may be made precise with relatively little calculation using a graph, which is similar to those for stability estimates for the stirred-tank reactor described by Regenass and Aris (1965).

Ishida and Wen (1968) proposed the concept of the *effectiveness factor* for noncatalytic solid-gas reaction, similar to that employed in a catalytic reaction. They discussed the effect of heat of reaction on the reaction rate, the types of instabilities occurring in a single particle, and the effects of system parameters on the overall rate, in terms of the effectiveness factor.

Ishida and Shirai (1969) presented a graphical solution for the noncatalytic solid-gas reaction system based on unreacted-core-shrinking model. They also studied the combustion of single carbon-cement sphere based on this model.

Luss and Amundson (1969) studied the temperature rise in a spherical pellet for a gas-solid diffusion-controlled reaction. It was found in general that the unreacted core has a uniform temperature distribution except in the initial stage of the reaction.

Beveridge and Goldie (1968) studied the transient heat transfer in a shrinking-core particle to give a more rationalized analysis of thermal instability.

MATHEMATICAL MODEL

The effects of heat of reaction and heat transfer in noncatalytic solid-gas reactions were analyzed previously based on the unreacted-core-shrinking model (Wen and Wang, 1970). The differences between pseudo steady state and unsteady state heat transfer analysis were also presented.

The material and heat balances have been derived for the nonisothermal unreacted-core-shrinking model (Wen and Wang, 1970). Referring to Figure 1, the pseudo steady state material balance and boundary conditions are

$$\frac{d^2x_A}{dr^2} + \frac{2}{r}\frac{dx_A}{dr} = 0 \quad r_c < r < R \tag{1}$$

$$r = R, \quad (CD_{eA})_{T_o}\frac{dx_A}{dr}\bigg|_{r=R} = (k_{mA}C)_{T_o}(x_{Ao} - x_{As}) \tag{2}$$

$$r = r_c, \quad (CD_{eA})_{T_o}\frac{dx_A}{dr}\bigg|_{r=r_c} = ak_{s(T_c)}C_{So}{}^m C_{Ac}{}^n \tag{3}$$

$$r = r_c, \quad (CD_{eA})_{T_o}\frac{dx_A}{dr}\bigg|_{r=r_c} = -aC_{So}\frac{dr_c}{dt} \tag{4}$$

$$t = 0, \quad r_c = R \tag{5}$$

The transient heat balance and boundary conditions are

$$\frac{\partial T}{\partial t} = \frac{k_e}{C_{pe}}\left(\frac{\partial^2 T}{\partial r^2} + \frac{2}{r}\frac{\partial T}{\partial r}\right) \quad r_c < r < R \tag{6}$$

$$r = R, \quad -k_e\frac{\partial T}{\partial r}\bigg|_{r=R} = h_C(T_s - T_o) + h_R(T_s{}^4 - T_w{}^4) \tag{7}$$

$$r = r_c, \quad 4\pi r_c{}^2 a k_{s(T_c)}C_{So}{}^m C_{Ac}{}^n(-\Delta H) + 4\pi r_c{}^2 k_e\frac{\partial T}{\partial r}\bigg|_{r=r_c} = \frac{4}{3}\pi r_c{}^3\rho_c C_{pc}\frac{dT_c}{dt} \tag{8}$$

$$t = 0, \quad T = T_c = T_i \tag{9}$$

The reaction occurring in the solid proceeds according to the scheme:

$$aA(\text{gas}) + S(\text{solid}) \rightarrow \text{Gas and/or Solid Product} \tag{10}$$

In Equation (8) it is assumed that the temperature within the unreacted core is uniform at T_c. The temperature dependency of the reaction rate constant is assumed to be of Arrhenius' type. The effectiveness factor is given by

$$\eta_s = \frac{k_{s(T_c)}C_{Ac}{}^n}{k_{s(T_o)}C_{Ao}{}^n} = \left(\frac{\omega_c}{U_c}\right)^n \exp\left[\frac{E}{\mathcal{R}T_o}\left(1 - \frac{1}{U_c}\right)\right] = -\frac{d\xi_c}{d\theta_s} \tag{11}$$

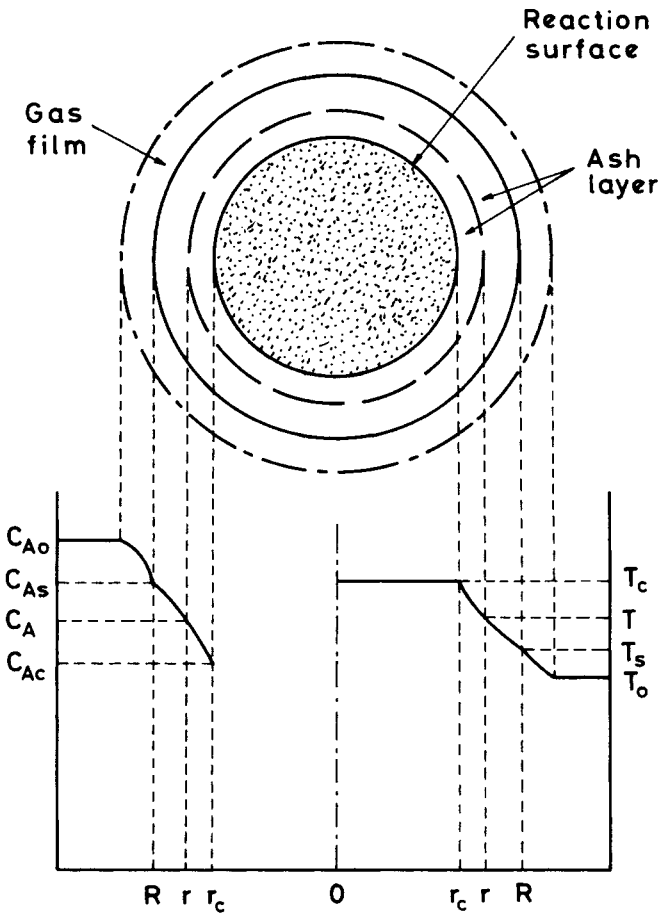

Fig. 1. Concentration and temperature profiles in an unreacted-core shrinking particle.

By assuming that the temperature distribution in the ash layer can be approximated at all times by a steady state profile, it is possible to reduce the above partial differential equations and their boundary conditions into a set of nonlinear ordinary differential equations (Wen and Wang, 1970). The IBM System/360 Continuous System Modeling Program (S/360 CSMP) has been used to solve this set of ordinary differential equations. The fourth-order variable-step Runge-Kutta integration method is used. A relative error of 10^{-4} is specified for integrator output for U_c and an absolute error of 10^{-4} for ξ_c.

EXPERIMENTAL EQUIPMENT

A schematic diagram of the thermobalance proper is shown in Figure 2. The heated section of the reactor is made of 43-in. long, 1½-in. schedule 40, type 310 stainless steel pipe. It is heated by three sections of "Thermoshell" electric heating elements; each section is 12-in. long, with a 1.9-in. inside diam. and is rated at 1200 watts/section. The bottom part of the reactor is packed with ½-in. Intalox saddle packings to a height of 15 in. for better heating and flow distribution of gas. The locations of thermocouples are also shown in Figure 2.

Figure 3 shows the equipment setup and temperature controls for the thermobalance. The temperatures at locations shown in Figure 2 are recorded by a Honeywell 12-point Electronik recorder at a rate of 5 cycles/min. or 1 point/sec. The weight of solid sample is continuously recorded by a "Mosely" Model 680 recorder.

Preparation of Solid Samples

Activated charcoal of USP grade was used as the solid reactant. Kaiser Refractories special prepared fire clay was used as an inert material in the solid particle. The absolute density as measured using a pycnometer was 1.637 g/cm³ for activated charcoal, and was 2.409 g/cm³ for fire clay after reaction.

The Tyler screen analyses indicated that 78 wt. % of activated charcoal powder was 200 ~ 400 mesh, while 82 wt. % of fire clay was 65 ~ 100 mesh.

The solid spheres used in the experiment were prepared by mixing a desired proportion of activated charcoal with fire clay which served as an inert porous medium. Proper amount of water was added into the powder mixture to form a well-mixed homogeneous thick slurry. A mold was then used to shape this thick slurry into balls of desired size. The balls were kept at room temperature to dry for about 10 to 14 days. After the spheres prepared in the same batch were dried, they were heated together under the nitrogen blanket in an oven to 815°C for at least 40 minutes. This procedure removed the moisture and other decomposable compounds from the solid sample. The fire clay is an impure form of kaolin and gives off water molecules at about 600°C according to the reaction

$$Al_2Si_2O_5(OH)_4 \rightarrow Al_2O_3 \cdot 2SiO_2 + 2H_2O$$

Thus, the heating of solid in nitrogen eliminated the weight loss of the solid sample due to side reactions during the test. After the particles were cooled, each lot was quickly sealed in a bottle with desiccant. The % carbon content in a particle for each lot was determined.

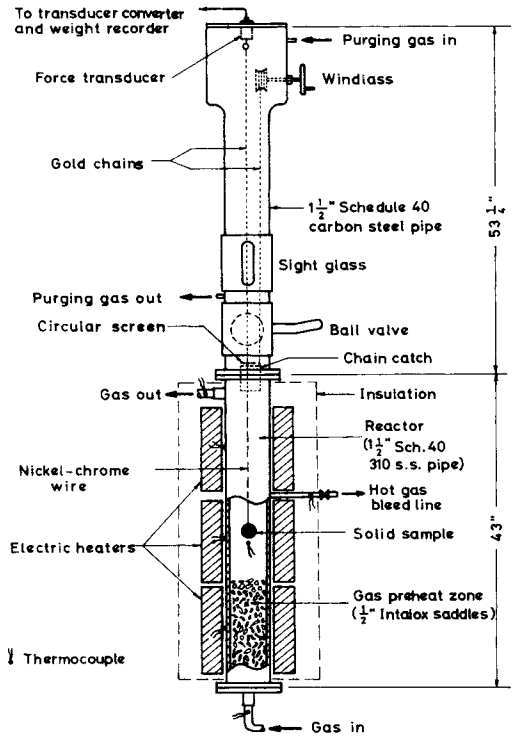

Fig. 2. Thermobalance proper.

EXPERIMENTAL PROCEDURE

Referring to Figures 2 and 3, the three sections of reactor heaters were first turned on with the temperatures set at the desired points by two temperature controllers (on-off and proportional). The bottom heater for the gas preheat zone was controlled by the proportional temperature controller. The on-off temperature controller controlled the temperature of the middle heater via a magnetic switch which turned on and off the electric current to both the top and middle heaters. However, the top heater temperature could be adjusted independently of the middle heater by powerstats. A thermocouple was located at a point approximately 6 mm below the solid particle. This thermocouple measured the apparent temperature at the reactor center T_{tc} which indicated a temperature between those of bulk gas and reactor wall. When no heat was generated inside the solid particle (that is, at the end of reaction), the particle temperature should be nearly the same as T_{tc}. The above method enabled the control of the temperature T_{tc} to within ± 2.8°C of the desired point.

With the ball valve closed, the desired air flow rate was established. The solid sample was hung from a piece of nickel-chrome wire which was attached to a gold chain located in the centerline of the reactor column. A windlass and another gold chain with a chain catch, located at off-centered position as shown in Figure 2, were used to raise and lower the sample by catching a circular screen attached to the center chain. When the system reached steady state conditions the sample was quickly lowered into the heated zone by unwinding the windlass.

To stop the reaction, the particle was raised into the cold upper section of the column, and the ball valve closed. This would effectively quench the reaction. An inert gas may be

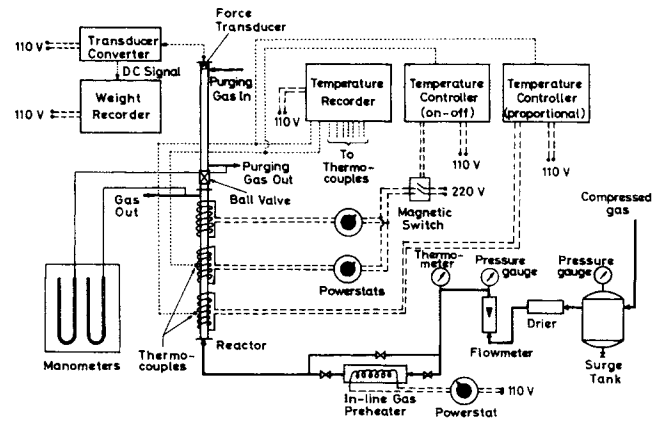

Fig. 3. Schematic diagram of equipment setup and temperature controls.

introduced into the upper section of the column, if necessary, to help quenching the reaction. The inert gas also served to prevent vapor condensation on the center gold chain during the reaction, when the reaction produced condensable vapors.

The solid particle was weighed on an analytical balance, both before and after the reaction.

Because of the difficulties in the simultaneous measurements of particle temperatures and weight changes, these measurements were carried out using duplicate and separate experiments.

EXPERIMENTAL AND CALCULATED RESULTS

Figure 4 shows the experimental results of two typical runs of particles containing 21.22 and 40.83% by wt. of carbon. The fractional conversions X of solid reactant (= weight loss/initial carbon content) are plotted against the reaction time. The calculated $t - X$ curves, based on the unsteady state heat transfer analysis of the model, are also plotted in the figure for comparison. The experimental surface reaction rates for these two runs, based on the unreacted-core type mechanism, are plotted against X in Figure 5. Calculated curves of surface reaction rate, using both the pseudo steady state ($A = 0$ and $G = 0$) and unsteady state heat transfer analyses, are also given in Figure 5. The surface reaction rates are equivalent to the effectiveness factors, being different only by a constant factor. The measured temperature variations with time at two points within the solid particle for these two runs are shown in Figures 6 and 7. The calculated curves by unsteady state heat transfer method are also shown.

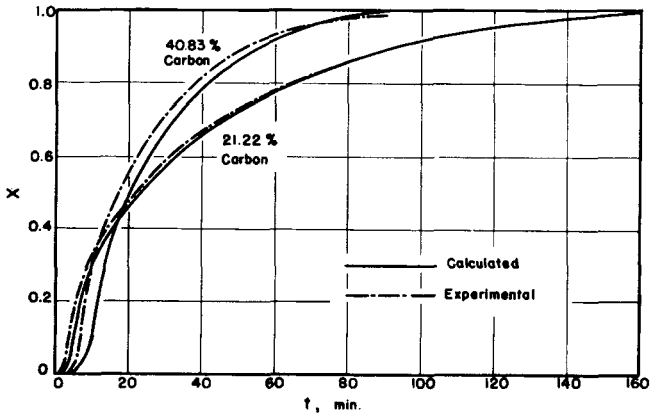

Fig. 4. Typical experimental and calculated time-conversion curves.

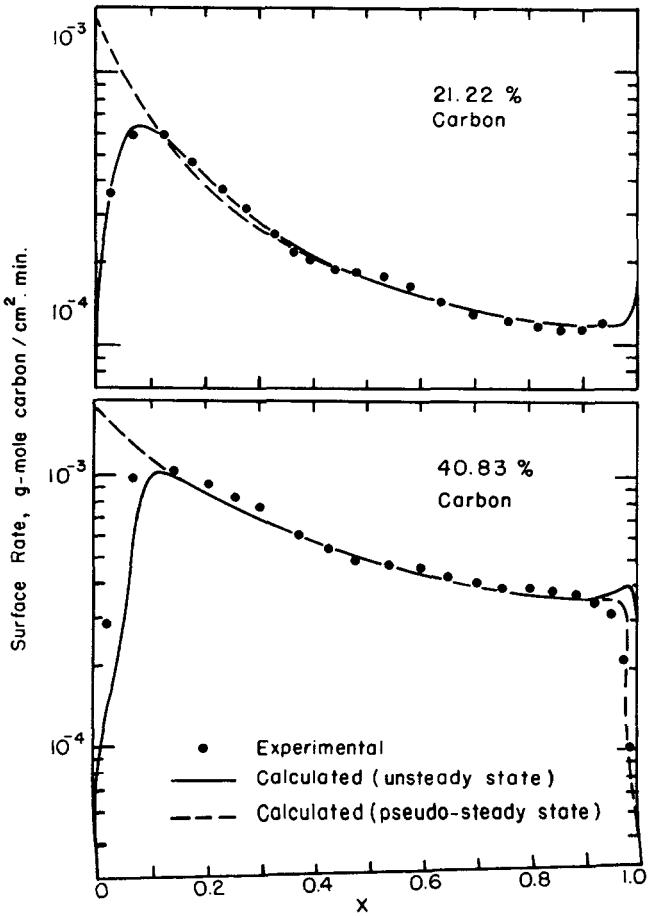

Fig. 5. Experimental and calculated surface rate-conversion curves.

The operating conditions and the physical and chemical properties used in the calculations of the theoretical curves in Figures 4 through 7 are listed in Table 1. The evaluations of some of the physical and chemical properties listed in Table 1 are given in the Appendix.*

SURFACE REACTION RATE CONSTANT AND EFFECTIVE DIFFUSIVITY

The rate constant values reported in the literature for carbon-oxygen reaction vary widely (see Figure A1, Appendix*). The rate of oxidation of carbon depends greatly on the types of carbon. The presence of impurities is known to affect the reaction rate, sometimes increasing the rate by orders of magnitude (Walker et al., 1959). However, the reported values of activation energy seem to fall within a narrow range around 40 kcal/g-mole. In a summary study by Satterfield (1970) on the oxidation of coke deposits on various catalysts and supports it was pointed out that the observed intrinsic activation energies for first-order reaction rate constants all fall between 35 and 40 kcal/g-mole. The oxidation rates, however, vary as many as 3 to 4 orders of magnitude.

Therefore, the surface reaction rate constant $k_{s(T_o)}$ was regarded as a parameter of the mathematical model for the carbon-oxygen reaction being considered, and the values of $k_{s(T_o)}$ for each run listed in Table 1 were obtained by the best fit of the calculated curves to the experimental

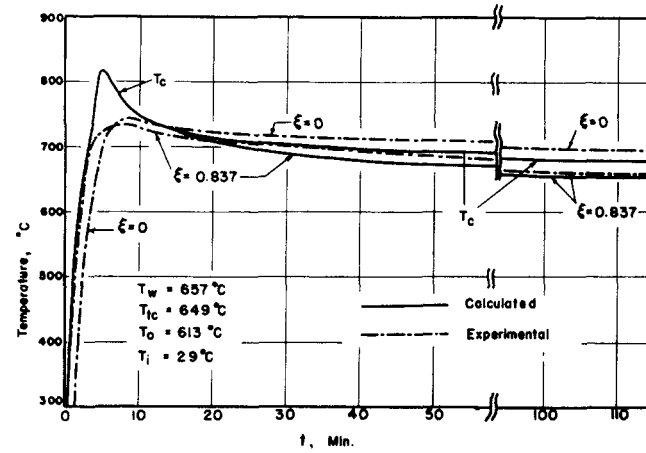

Fig. 6. Experimental and calculated time-temperature curves for low-carbon run.

* The Appendix has been deposited as Document No. 01922 with the National Auxiliary Publications Service (NAPS), c/o CCM Information Corp., 866 Third Ave., New York 10022 and may be obtained for $2.00 for microfiche or $5.00 for photocopies.

results. However, an activation energy of 37.5 kcal/g-mole was used for both runs.

When the overall reaction rate is controlled by the ash layer diffusion, an accurate value of D_{eA} must be used in the computer simulation of experimental result. Theoretical or empirical correlations are available in the literature for the estimation of effective diffusivity (Satterfield, 1970; Shirotsuka et al., 1970; Wakao and Smith, 1962; Youngquist, 1970). However, no correlation can be used with reasonable confidence because the effective diffusivity depends greatly on the characteristics of solid structure such as pore size, porosity, tortuosity, etc.

Therefore, a diffusivity apparatus, similar to that used by Socony Mobil Oil Company (Mobil Method 366-59), was used to measure directly the effective diffusivity of ash layer for the binary system of O_2 and N_2. A sample of the test solid was placed in a diffusion cell between gas streams of different compositions. The gas streams on both sides of the sample were maintained at room temperature and atmospheric pressure. Concentrations of the effluent streams were determined by a gas chromatograph after steady state had been reached. Since the gas mixture contained approximately 80 mole % of nitrogen under the reactor condition, it was assumed that $D_{eA} = D_{e,\ O_2\text{-mixture}} \cong D_{e,\ O_2\text{-}N_2}$.

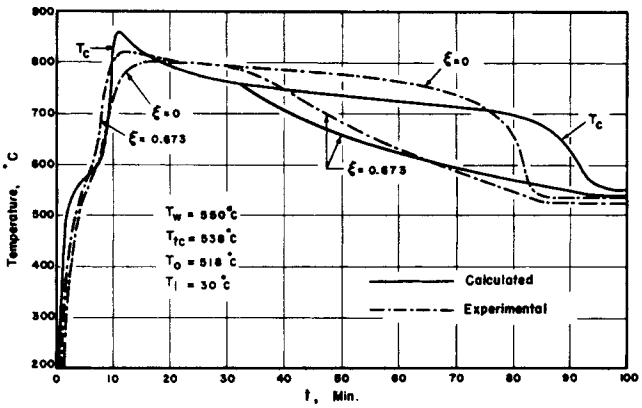

Fig. 7. Experimental and calculated time-temperature curves for high-carbon run.

TABLE 1. OPERATING CONDITIONS AND PHYSICAL AND CHEMICAL PROPERTIES USED IN FIGURES 4 THROUGH 7

Carbon content, % by weight	21.22	40.83
R, cm	1.210	1.230
Ash layer porosity, ϵ	0.566	0.750
Ash layer bulk density, gm/cc	1.046	0.601
Porosity of unreacted particle, ϵ_o	0.394	0.497
C_{So}, g-mol carbon/cc	0.0235	0.0345
C_{Ao}, g-mol oxygen/cc @ T_o	3.41×10^{-6}	3.80×10^{-6}
Temperatures, °K: T_o	886	791
T_{tc}	886	791
T_w	930	823
*D_{fA}, cm²/s @ T_o	1.11	0.916
$D_{eA}(T_o)$, cm²/s	0.238	0.430
v, cm/s	198.5	181.2
N_{Re}, particle	600	669
*h_C, cal/s-cm²-°C	9.18×10^{-4}	8.78×10^{-4}
*h_R, cal/s-cm²-°K⁴	8.94×10^{-13}	8.54×10^{-13}
*$k_{mA}(T_o)$, cm/s	6.94	5.94
*k_e, cal/s-cm-°C	1.48×10^{-3}	7.10×10^{-4}
*Stoichiometric coefficient, a	0.83	0.75
C_{pe}, cal/°C-cm³ of ash layer	0.241	0.128
C_{pc}, cal/°C-gm of core	0.247	0.263
ρ_c, gm/cm³ of core	1.327	1.016
*E, kcal/g-mol	37.5	37.5
*$k\,s(T_o)$, cm/s ($m = 0, n = 1$)	0.34	0.115

* See Appendix.

TABLE 2. AVERAGE MEASURED EFFECTIVE DIFFUSIVITIES AT 25°C AND 1 ATM.
($D_{fA} = 0.207$ cm²/s at 25°C)

Average porosity	0.439	0.568	0.665	0.750
D_{eA}/D_{fA}	0.110	0.183	0.266	0.402
No. of measurements	6	6	6	7
Standard deviation, %	7.3	8.3	15.6	14.7

The solid sample of ash layer of fire clay was cut into a cylindrical shape, at random orientation, of approximately 0.36 cm in diam. and 0.55 cm in length. No evidence of the anisotropic effect of solid structure was observed in the measured results.

Table 2 gives the summary of the measured effective diffusivities in terms of the ratios to molecular diffusivities. The measured effective diffusivities were calculated, based on nonequimolar steady state counterdiffusion for binary mixture (Satterfield, 1970; Youngquist, 1970), from O_2 concentrations determined by a gas chromatograph.

In order to determine whether the ash layer diffusion was in the Knudsen diffusion or molecular diffusion regime, it was necessary to find the mean pore radius of the ash layer of fire clay. Table 3 gives the surface areas of some typical ash layers of fire clay measured by Brunauer-Emmett-Teller method. The mean pore radii, calculated from the pore volume and surface area by assuming cylindrical pores, are also given in Table 3. The calculated mean free paths of gas molecules (Perry et al., 1963) are in the order of 2700Å at the reactor condition. By comparing the mean pore radii and the mean free paths it can be concluded that the diffusion in the ash layer having porosity of 0.748 (41% carbon) and $\bar{r} = 3677$Å is by molecular diffusion. The diffusion in lower porosity ash layers ($\epsilon = 0.442$, 0.570, and 0.665) may be slightly affected by Knudsen diffusion, especially at high reactor temperature.

Having established that the ash layer diffusion is predominantly in the molecular regime, the effective diffusivities at the reactor conditions can be obtained by extrapolation from the measured room temperature values, using a temperature dependency factor of $T^{1.69}$ for molecular diffusion (Equation A1).

Figure 8 shows the effective diffusivities (in solid lines) obtained by extrapolation from measured room temperature values given in Table 2. The dashed line for $\epsilon = 1.0$ is calculated from Equation (A1) for molecular diffusivity.

In order to verify that such extrapolation was valid, some effective diffusivities were calculated from the reaction rates of experimental runs which were ash diffusion controlled. The following equation was used:

$$(CD_{eA})\left.\frac{dx_A}{dr}\right|_{r=r_c} = -aC_{So}\frac{dr_c}{dt}$$

where $-C_{So}\dfrac{dr_c}{dt}$ is the reaction rate, and the rate at $\xi_c = 0.8$ ($X = 0.488$) was used. The reasons for selecting the rate at $\xi_c = 0.8$ were to ensure that the ash diffusion was rate controlling and the ash layer was still thin enough to be approximated as a slab. Also, the reaction temperature T_c was fairly constant by the time $\xi_c = 0.8$ was reached. Since the air flow rate was high for these runs, the concentration of oxygen at particle surface could be approximated by x_{Ao}. The oxygen concentration at reaction interface was

Table 3. Surface Area and Mean Pore Radius of Ash Layer of Fire Clay

Porosity ϵ	0.442	0.570	0.665	0.748
Surface area S_g, m²/gm	17.17	15.72	19.07	6.706
Bulk density ρ_{bulk}, gm/cc	1.345	1.037	0.806	0.607
Pore volume $V_g = \frac{\epsilon}{\rho_{bulk}}$, cc/gm	0.328	0.550	0.826	1.233
Mean pore radius $\bar{r} = \frac{2V_g}{S_g}$, A	382	700	866	3677

negligible ($x_{Ac} = 0$). Hence,

$$-aC_{So}\frac{dr_c}{dt} \cong (CD_{eA})\frac{x_{Ao}}{R - r_c}$$

or

$$D_{eA} \cong \frac{(0.2)RaRT\left(-C_{So}\frac{dr_c}{dt}\right)}{(0.2095)\ P} \qquad (12)$$

The value for a in Equation (12) is found from Equations (A2) and (A3). An arithmetic average of $(T_s + T_c)/2$, where T_s was approximated by T_{tc}, was used in Equation (12). The results are plotted in Figure 8 as data points.

It is seen that the data points agree well with the extrapolated values (solid lines) when the porosities are high. The extrapolated values tend to be high for low porosities. This may be due to the effect of Knudsen diffusion as mentioned earlier. Also, the data points at low temperatures (around 650°C) tend to be slightly low, resulting in a somewhat higher slope than the extrapolated lines. This is probably due to the assumption of $x_{Ac} = 0$, whereas in actuality it may not be zero, though small, at low temperature. Thus, if a more realistic driving force, a lower value of $x_{Ao} - x_{Ac}$, had been used in Equation (12) the agreement would have been better.

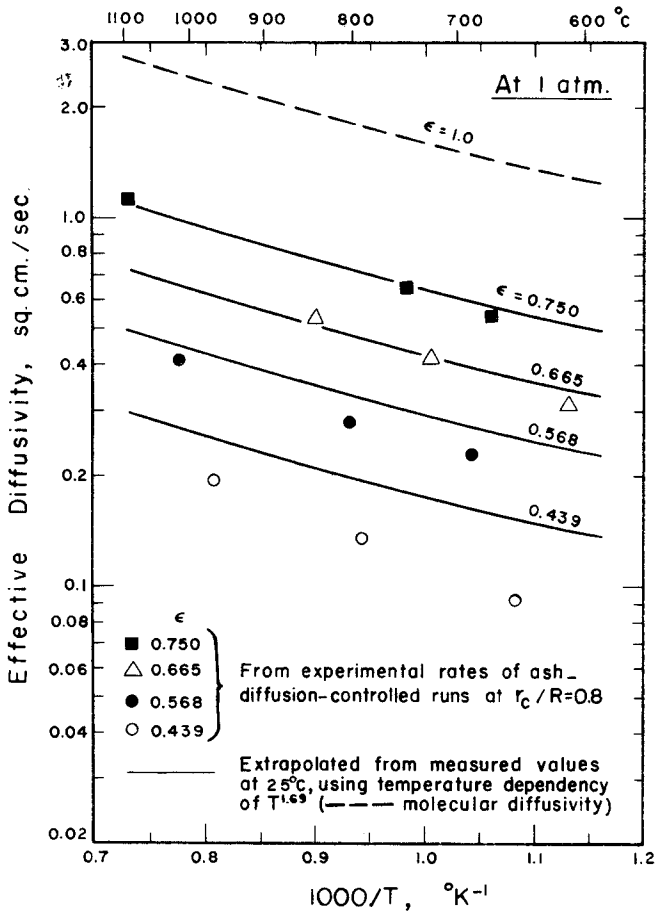

Fig. 8. Effective diffusivities in the ash layer of fire clay.

The good agreement between the effective diffusivity, obtained from the reaction rate and Equation (12), and that extrapolated from the actual measurement is direct evidence that the unreacted core-shrinking model is valid for the reaction system being considered, when the ash diffusion is rate controlling.

The values of $D_{eA(T_O)}$ listed in Table 1 were obtained by extrapolation from the measured room temperature values (solid lines in Figure 8).

COMPARISON AND DISCUSSION OF RESULTS

All the experimental runs conducted at reactor temperature (T_{tc}) equal to or above 800°K produced sharp reaction interface; an evidence visually observed by cutting the solid sphere into two halves. At about 755°K or lower, the particle started to show zone type reaction. The two typical runs shown in Figures 4 through 7 were observed to follow the unreacted core-shrinking type phenomenon shown in Figure 1.

Figure 4 shows that the calculated and experimental $t - X$ curves agree well when the carbon content of the solid particle is low at 21% (see Table 1, low-carbon run). However, the two curves deviate significantly from each other when the carbon content is high at 41% (high-carbon run). In general, the deviation is greater during the initial stage of reaction.

This deviation is due to the assumption that the temperature within the unreacted core is uniform and equal to reaction temperature T_c at all times. This assumption is valid when the thermal diffusivity of the unreacted core is very large, or when the particle temperature does not change greatly with time. Since the unreacted core does not have a very large thermal diffusivity and the initial particle temperature is low at room temperature, the heat of reaction generated during the initial period will create a large temperature gradient within the particle. Therefore, the actual conversion during the initial stage will be faster than that calculated. Once the temperature at the center of the particle reaches the reaction temperature, the assumption is valid.

The discrepancy between the actual and calculated reaction temperatures can be greatly reduced, however, by preheating the solid particle in an inert gas to the reactor temperature before its entry to the reactor. This would avoid the large temperature gradient within the particle during the initial stage.

Figure 5 shows the variation of the surface reaction rate with the fractional conversion of carbon, assuming the unreacted-core type reaction. It is seen that the unsteady state heat transfer analysis describes the experimental results better than the pseudo steady state analysis. Again, owing to the assumption of uniform temperature within the unreacted core, the calculated rates (unsteady state analysis) are lower than the experimental values during

the initial period of reaction. The difference is more pronounced for the particle with a higher carbon content due to its large amount of heat generated, producing a sharp temperature gradient.

Figure 5 also shows that the transitional instability occurred at solid conversion of about 95% for the high-carbon run. The transition was gradual (the pseudo steady state solution having only one root) from diffusion-controlled regime to chemical-reaction-controlled regime.

Three types of instability, that is, geometrical instability, thermal instability due to metastable temperature, and sudden transition of the rate controlling steps, were discussed previously (Aris, 1967; Beveridge and Goldie, 1968; Cannon and Denbigh, 1957; Ishida and Wen, 1968; Regenass and Aris, 1965; Shen and Smith, 1965; Wen and Wang, 1970). In the present experimental study a fourth type of instability was found to be possible, as shown in Figure 5 for 40.83% carbon. This type of instability occurs when the relative positions of the heat loss and heat generation curves are such that only one crossing point is possible, as shown schematically in Figure 9 (Wang, 1971). This usually occurs when the heat loss line has large slope (high heat loss rate). When the crossing point shifts from the diffusion regime to kinetic regime during the course of reaction as shown by path $A \rightarrow B \rightarrow C \rightarrow D \rightarrow E$ in Figure 9, the extinction is gradual in the sense that the crossing point moves down along the sigmoid curve and does not abruptly shift as in the case of the sudden transition. At any time during the gradual transition, the following conditions are satisfied at the crossing point:

$$Q_{gen} = Q_{loss}$$

$$\frac{\partial Q_{gen}}{\partial T_c} < \frac{\partial Q_{loss}}{\partial T_c}$$

Two thermocouples were used to measure the temperature variations within a particle: One 1.59 mm diameter thermocouple located at the center, and one 0.508 mm diameter located a few millimeters deep from the surface. Figures 6 and 7 show the measured and calculated temperature curves. The measured temperature at the center of particle reached a peak value which was lower and occurred a few minutes later than the calculated peak reaction temperature T_c. According to the assumption of uniform unreacted core temperature the measured center temperature should be the same as the reaction temperature. Also, the off-centered thermocouple should register the same reaction temperature if it was still within the unreacted core. In actuality, however, these situations happened only after a certain reaction time had elapsed.

The disagreement in time scale, when the calculated T_c and the measured temperature at particle center drop sharply (gradual extinction) in Figure 7, may be a result of errors introduced by using separate and duplicate experiments for temperature and weight change measurements. However, the disagreement of 10 minutes as in Figure 7 corrsponds to an error of less than 1.5% of solid conversion at conversion level of over 95%. As indicated previously, the values of $k_{s(T_0)}$ for each run listed in Table 1 were obtained when the experimental data were best fitted. From these values, the frequency factors, after dividing by the carbon concentration C_{So}, are calculated as $k_s^0 \times 10^{-10} = 2.58$ and 7.60 cm⁴/gmol-sec for low and high-carbon runs, respectively. The value for the low-carbon run may be less accurate because of larger diffusion effect at higher operating temperature and lower porosity of the ash layer. Nevertheless, the agreement in the frequency factors is good. Using an average value of 5.1×10^{10} cm⁴/gmol-sec for k_s^0, and $E = 37.5$ Kcal/gmol, the Arrhenius plot for the carbon-oxygen reaction in this study is represented by curve 4 in Figure A1 for comparison with literature values.

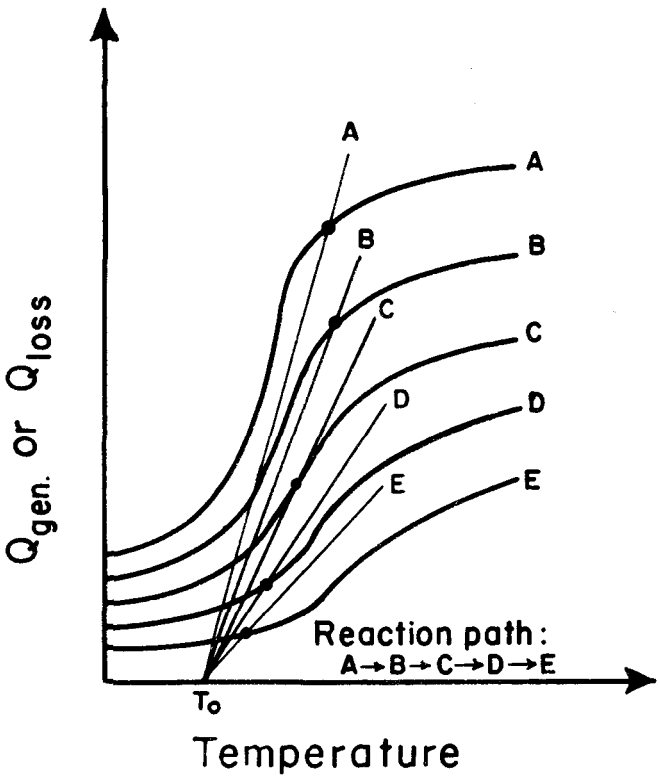

Fig. 9. Relation between heat generation and heat loss curves in a gradual transition of rate controlling regimes.

ACKNOWLEDGMENT

This project was partially supported by the National Science Foundation Enrichment Fund.

NOTATION

- a = stoichiometric coefficient
- A = $C_{Ao}D_{eA(T_0)}C_{pe}/aC_{So}k_e$, ratio of mass to thermal diffusivities in ash layer
- C = total concentration of gases, mole/L³
- C_A = concentration of gaseous reactant A in ash layer, C_{Ac} at unreacted-core surface, C_{Ao} in bulk gas phase, C_{As} at outer surface of particle, mole/L³
- C_{pc} = heat capacity of unreacted core, H/MT
- C_{pe} = volumetric heat capacity of ash layer, H/L³T
- C_S = concentration of solid reactant S, C_{So} initial concentration, mole/L³
- d_p = diameter of particle, L
- D_{eA} = effective diffusivity of component A in ash layer, L²/θ
- D_{fA} = molecular diffusivity of component A, L²/θ
- E = activation energy of reaction rate constant, H/mole
- G = $\rho_c C_{pc} T_o/aC_{So}(-\Delta H)$, ratio of enthalpy of unreacted core to heat of reaction
- h_C = convective heat transfer coefficient, H/L²θT
- h_R = radiational heat transfer coefficient, H/L²θT^4
- ΔH = heat of reaction per mole of gaseous reactant A, H/mole
- k_e = effective thermal conductivity of ash layer, H/LθT

k_f = thermal conductivity of bulk gas, $H/L\theta T$
k_{mA} = mass transfer coefficient of component A across gas film, L/θ
k_s = surface reaction rate constant based on solid reactant, $L^{3(m+n)-2}/mole^{m+n-1}\theta$
k_s^0 = frequency factor for surface reaction rate constant, $L^{3(m+n)-2}/mole^{m+n-1}\theta$
m = order of reaction for solid reactant
n = order of reaction for gaseous reactant
N_{Pr} = Prandtl number
N_{Re} = particle Reynolds number based on velocity v
N_{Sc} = Schmidt number
P = total pressure, F/L^2
Q_{gen} = heat generation rate per particle, H/θ
Q_{loss} = heat loss rate per particle, H/θ
r = distance from center of sphere, L
$\bar{r}$ = mean pore radius, L
r_c = radius of unreacted core, L
R = particle radius, L
$\mathcal{R}$ = gas constant, H/mole T
t = time, θ
T = temperature, T_c at unreacted-core surface, T_i initial particle temperature, T_o at bulk gas phase, T_s at outer surface of particle, T_{tc} apparent temperature at center of reactor, T_w at reactor wall, T
U_c = T_c/T_o
v = gas velocity based on annular cross-sectional area between reactor wall and solid particle, L/θ
x_A = mole fraction of component A, x_{Ac} at unreacted-core surface, x_{Ao} in bulk gas phase, x_{As} at outer surface of particle
X = fractional conversion of solid reactant S ($= 1 - \xi_c^3$)

Greek Letters

ϵ = porosity of ash layer, ϵ_o of unreacted particle
η_s = effectiveness factor based on surface reaction
θ_s = $k_{s(T_o)}C_{Ao}{}^nC_{So}{}^{m-1}t/R$
ξ = r/R
ξ_c = r_c/R
ρ_c = density of unreacted core, M/L^3
ω_c = x_{Ac}/x_{Ao}

LITERATURE CITED

Aris, R., "Transition between Regimes in Gas-Solid Reactions," *Ind. Eng. Chem. Fundamentals*, **6**, 315 (1967).

Beveridge, G. S. G., and P. J. Goldie, "Effectiveness Factors and Instability in Non-Catalytic Gas-Solid Reactions: the Effect of Solid Heat Capacity," *Chem. Eng. Sci.*, **23**, 913 (1968).

Bird, R. B., W. E. Stewart, and E. N. Lightfoot, Transport Phenomena, p. 647, Wiley, New York (1960).

Cannon, K. J., and K. G. Denbigh, "Studies on Gas-Solid Reactions, Parts I & II," *Chem. Eng. Sci.*, **6**, 145, 155 (1957).

Costa, E. C., and J. M. Smith, "Kinetics of Noncatalytic, Non-isothermal, Gas-Solid Reaction: Hydrofluorination of Uranium Dioxide," *AIChE J.*, **17**, 947 (1971).

Field, M. A., D. W. Gill, B. B. Morgan, and P. G. W. Hawksley, Combustion of Pulverised Coal, Br. Coal Utilisation Research Assn., Leatherhead, Surrey, England (1967).

Francl, J., and W. D. Kingery, "Thermal Conductivity: IX, Experimental Investigation of Effect of Porosity on Thermal Conductivity," *Am. Ceramic Soc. J.*, **37**, 99 (1954).

Frank-Kamenetskii, D. A., Diffusion and Heat Transfer in Chemical Kinetics, 2nd ed., Plenum Press, New York (1969).

Froessling, N., "Evaporation of Falling Droplets," *Gerlands Beitr. Geophys.*, **52**, 170 (1938).

Golovina, E. S., and G. P. Khaustovich, "The Interaction of Carbon with Carbon Dioxide and Oxygen at Temperatures up to 3000°K," 8th Intern. Symp. on Combustion, pp. 784-792 (1962).

Hughmark, G. A., "Mass and Heat Transfer from Rigid Spheres," *AIChE J.*, **13**, 1219 (1967).

Ishida, M., and T. Shirai, "Graphical Representation of Solid-Gas Reactions Based on Unreacted Core Model," *Chem. Eng. J.*, (Japan) **2**, 175 (1969).

———., "Non-Isothermal Analysis of Unreacted-Core Model for the Burning Rate of Single Carbon-Cement Spheres," *ibid.*, 180.

Ishida, M. and C. Y. Wen, "Comparison of Kinetic and Diffusional Models for Solid-Gas Reactions," *AIChE J.*, **14**, 311 (1968).

———., "Effectiveness Factors and Instability in Solid-Gas Reactions," *Chem. Eng. Sci.*, **23**, 125 (1968).

Kunii, D., and J. M. Smith, "Heat Transfer Characteristics of Porous Rocks," *AIChE J.*, **6**, 71 (1960).

Levenspiel, O., Chemical Reaction Engineering, Ch. 12, Wiley, New York (1962).

Luss, D., and N. R. Amundson, "Maximum Temperature Rise in Gas-Solid Reactions," *AIChE J.*, **15**, 194 (1969).

Nagle, J., and R. F. Strickland-Constable, "Oxidation of Carbon between 1000 ~ 2000°," *Proc. 5th Conf. on Carbon*, **1**, 154 (1962).

Norton, F. H., Refractories, 3rd ed., p. 508, McGraw-Hill, New York (1949).

Ogawa, Y., *Tech. Rep.*, Tohoku Imperial Univ., 9, 175 (1929).

Parker, A. S., and H. C. Hottel, "Combustion Rate of Carbon, Study of Gas-Film Structure by Microsampling," *Ind. Eng. Chem.*, **28**, 1334 (1936).

Perry, R. H., C. H. Chilton, and S. D. Kirkpatrick, Chemical Engineers' Handbook, 4th ed., McGraw-Hill, New York (1963).

Ranz, W. E., and W. R. Marshall, "Evaporation from Drops, Parts I & II, *Chem. Eng. Progr.*, **48**, 141, 173 (1952).

Regenass, W., and R. Aris, "Stability Estimates for the Stirred Tank Reactor," *Chem. Eng. Sci.*, **20**, 60 (1965).

Rossberg, M., "Experimentelle Ergebnisse über die Primärreaktionen bei der Kohlenstoffverbrennuing," *Z. Elektrochemie*, **60**, 952 (1956).

Satterfield, C. N., Mass Transfer in Heterogeneous Catalysis, M.I.T. Press, Cambridge, Mass. (1970).

Shen, J., and J. M. Smith, "Diffusional Effects in Gas-Solid Reactions," *Ind. Eng. Chem. Fundamentals*, **4**, 293 (1965).

Shirotsuka, T., T. Togami, and I. Yokoyama, "Effective Diffusivity in Porous Media," *Kagaku Kogaku*, **34**, 1079 (1970).

Tu, C. M., H. Davis, and H. C. Hottel, "Combustion Rate of Carbon, Combustion of Spheres in Flowing Gas Streams," *Ind. Eng. Chem.*, **26**, 749 (1934).

Wakao, N., and J. M. Smith, "Diffusion in Catalyst Pellets," *Chem. Eng. Sci.*, **17**, 825 (1962).

Walker, P. L., Jr., F. Rusinko, Jr., and L. G. Austin, Advances in Catalysis, Vol. XI, p. 133, Academic Press, New York (1959).

Walls, J. R., and R. F. Strickland-Constable, "Oxidation of Carbon Between 1000 and 2400°," *Carbon*, **1**, 333 (1964).

Wang, S. C., "Reaction Kinetics in Noncatalytic Solid-Gas Systems," Ph.D. dissertation, West Virginia Univ., Morgantown (1971).

Weisz, P. B., and R. D. Goodwin, "Combustion of Carbonaceous Deposits within Porous Catalyst Particles, I. Diffusion-Controlled Kinetics," *J. Catalysis*, **2**, 397 (1963).

———., "Combustion of Carbonaceous Deposits within Porous Catalyst Particles, II Intrinsic Burning Rate," *ibid.*, **6**, 227 (1966).

Wen, C. Y., and S. C. Wang, "Thermal and Diffusional Effects in Non-Catalytic Solid Gas Reactions," *Ind. Eng. Chem.*, **62** (8), 30 (1970).

Wen, C. Y., "Noncatalytic Heterogeneous Solid Fluid Reaction Models," *ibid.*, **60** (9), 34 (1968).

Yagi, S., and D. Kunii, *5th Intern. Symp. on Combustion*, p. 231, Reinhold, New York (1955).

Youngquist, G. R., "Diffusion and Flow of Gases in Porous Solids," *Ind. Eng. Chem.*, **62** (8), 52 (1970).

Manuscript received February 11, 1972; revision received June 29, 1972; paper accepted July 5, 1972.